Systematic Study of the Embedding Potential Description in the Fragment Molecular Orbital Method†

Dmitri G. Fedorov,*,‡ Lyudmila V. Slipchenko,§ and Kazuo Kitaura‡,||

Research Institute for Computational Sciences (RICS), National Institute of Advanced Industrial Science and Technology (AIST), 1-1-1 Umezono, Tsukuba, Ibaraki 305-8568, Japan, Department of Chemistry, Purdue University, West Lafayette, Indiana 47907, USA, and Graduate School of Pharmaceutical Sciences, Kyoto University, Sakyo-ku, Kyoto 606-8501, Japan

Received: February 25, 2010; Revised Manuscript Received: April 11, 2010

We analyzed the accuracy of the fragment molecular orbital method using various representations of the embedding potential and extended its applicability to large basis sets by proposing to use potential-derived point charges with screening combined with the adaptive frozen orbital treatment of the detached bonds. A comprehensive set of basis sets: STO-3G, 6-31G*, 6-311G*, 6-31++G**, 6-311++G**, cc-pVDZ, cc-pVTZ, aug-cc-pVDZ, and aug-cc-pVTZ was employed; for tests systems we used water clusters with 16 and 32 molecules, the α-helices and β-strands of alanine containing 10 and 20 residues, as well as chignolin (PDB: 1UAO) and Trp-cage miniprotein (PDB: 1L2Y).

1. Introduction

Recently, there has been considerable development in the field of quantum-chemical methods applicable to large systems. On the one hand, there are traditional ab initio and semiempirical methods taking advantage of various ideas to reduce the scaling;[1–11] on the other hand, there are numerous fragment-based approaches.[12–28] In addition, new generation force fields based on quantum-chemical calculations of fragments have also been suggested.[29,30]

The fragment molecular orbital (FMO) method has been proposed by Kitaura et al.[31] extending the physical picture given by the energy decomposition analysis (EDA)[32] into the treatment of large systems by defining fragments and describing the interaction between them. FMO[33–35] has been developed to treat many types of wave functions[36–43] and their combinations in the multilayer approach[44] as well as solvent effects.[45,46] Geometry optimizations[47] and molecular dynamics[48–50] can be performed, as well as the fragment interaction analyses.[51–53]

FMO has been applied to an extensive number of problems, such as protein−ligand binding,[54,55] protein−DNA interaction,[56] explicit[57–60] and continuum[61] solvation, enzymatic reactions,[62] protein folding,[63] nanowires,[64] excited states in proteins,[65–67] and drug-design related studies.[68,69]

The distinctive feature of FMO is the inclusion of the electrostatic field from the whole system (sometimes called the embedding potential) into each individual fragment calculation, and in using the many-body expansion[70] to include the inter-fragment interactions.

The focus of the present work is to systematically study the representations of the embedding potential in FMO, which we call the electrostatic potential (ESP). ESP from the beginning has been described in FMO by the rigorous Coulomb potential consisting of the one- and two-electron terms, only approximated at large distances by point charges.[71] It has been shown[72] that the addition of the exchange interaction to ESP leads to very poor accuracy in FMO, except in the post factum construction of the total Fock matrix, which is done to obtain the molecular orbitals of the whole system. In a related study by Söderhjelm et al.,[73] several electrostatic models have been compared, and it has been pointed out that using the exact potential leads to some errors caused by the lack of the exchange-repulsion.

We now consider replacing all two-electron terms by point charges, even at short distances, and demonstrate that by doing so one can obtain reasonable accuracy for large basis sets, which is otherwise impossible with the rigorous ESP. Some previous studies also have reported the use of point charges in molecular clusters to describe ESP in FMO[42] and other related methods.[12,13] The performance of point charges can be improved with the point multipole screening,[74] which we apply in this work to ESP in FMO.

The covalent bond detachment in FMO can be performed in two ways: the hybrid orbital projection operator (HOP),[75] which is fully variational imposing no restrictions upon the fragment density distribution, and the adaptive frozen orbital approach (AFO),[76] which introduces frozen orbitals to describe detached bonds. The first has been typically applied to highly polar systems such as proteins, whereas the latter has been used in nanowires and zeolites. It has also been found that AFO works better with large basis sets by constraining the polarization (because the electron density of the detached orbitals is frozen). We use both schemes to evaluate the performance of potentials.

2. Computations

2.1. Methodology. The two-body FMO expansion (FMO2) is given for N fragments by

$$E^{\mathrm{FMO2}} = \sum_{I}^{N} E_I + \sum_{I>J}^{N} \Delta E_{IJ} \qquad (1)$$

where the total energy E of the full system is written as the sum of the monomer energies E_I, and the pair corrections

† Part of the "Klaus Ruedenberg Festschrift".

* To whom correspondence should be addressed. E-mail: d.g.fedorov@aist.go.jp.

‡ National Institute of Advanced Industrial Science and Technology.

§ Purdue University.

|| Kyoto University.

10.1021/jp101724p
Published on Web 05/05/2010

$\Delta E_{IJ} = E_{IJ} - E_I - E_J$, where E_{IJ} is the energy of the dimer made of two fragments I and J. To obtain a better accuracy, one can define the three-body FMO expansion (FMO3),

$$E^{\mathrm{FMO3}} = E^{\mathrm{FMO2}} + \sum_{I>J>K}^{N} \{(E_{IJK} - E_I - E_J - E_K) - \Delta E_{IJ} - \Delta E_{JK} - \Delta E_{KI}\} \quad (2)$$

which includes the triple corrections computed from the trimer energies E_{IJK}. Practically, in FMO each fragment calculation is performed in the field due to all other fragments until self-consistency (this procedure is known as the self-consistent charge, SCC), after which dimer, and, optionally, trimer calculations are done in the field of other fragments determined in SCC.

Individual n-mers (X) energies are obtained from doing their ab initio calculations, where the ab initio internal Hamiltonian H^{X} is modified by the addition of ESP V^X (X is monomer I, dimer IJ, or trimer IJK, for $n = 1$, 2, and 3, respectively),

$$V^X_{\mu\nu} = \sum_{K\neq X}^{N} \left\{ \sum_{A\in K} \left\langle \mu \left| -\frac{Z_A}{|\mathbf{r} - \mathbf{R}_A|} \right| \nu \right\rangle + \sum_{\rho\sigma\in K} D^K_{\rho\sigma}(\mu\nu|\rho\sigma) \right\} \quad (3)$$

The electrostatic potential has a one-particle form and is a straightforward matrix element of the Coulomb operator, describing the attraction between the electron density of X and nuclei of fragments $K \neq X$, and the corresponding repulsion between the electron density distributions of X and K. The nucleus−nucleus repulsion energy is added directly to the total energy. μ, ν, ρ, and σ run over atomic orbitals in X; K runs over $N-n$ fragments not included in X (n in n-mer X is defined above eq 3). Z_A and $\mathbf{R}_A$ are charges and coordinates of atoms A, respectively. $\mathbf{D}^K$ is the density matrix of fragment K.

This potential rigorously describes the Coulomb interaction between fragments, and it was shown[52] that it reproduces the exact electrostatic interaction (FMO vs unfragmented ab initio calculations), because of the many-body polarization taken into account in SCC. We denote the potential in eq 3 including two-electron terms as ESP2. One can approximate those terms as

$$\sum_{\rho\sigma\in K} D^K_{\rho\sigma}(\mu\nu|\rho\sigma) \approx \sum_{A\in K} \left\langle \mu \left| \frac{P_A}{|\mathbf{r} - \mathbf{R}_A|} \right| \nu \right\rangle \quad (4)$$

where P_A are atomic populations. Then the potential can be written using $q_A = Z_A - P_A$ as

$$V^X_{\mu\nu} = \sum_{K\neq X}^{N} \sum_{A\in K} \left\langle \mu \left| -\frac{q_A}{|\mathbf{r} - \mathbf{R}_A|} \right| \nu \right\rangle \quad (5)$$

This potential can be used with various ways of defining the atomic charges q_{A}. We compare the performance of the Mulliken (m) and potential-derived (p) charges determined on the fly from the fragment densities which mutually polarize each other in FMO self-consistently, denoting the corresponding potentials (eq 5) as ESPm and ESPp, respectively. In practice, in ESP2 the contributions to the potential from remote fragments are also approximated according to eq 4 (which introduces very little error) using the point charges (the effect of the charge definition upon far separated interaction is very small).

The Mulliken charges[77] are given by

$$q^X_I = -\sum_{A\in I} P^X_A + Z_I$$
$$P^X_A = \sum_{\mu,\nu\in A} D^X_{\mu\nu} S^X_{\mu\nu} + \frac{1}{2} \sum_{\mu\in A} \sum_{\nu\notin A} D^X_{\mu\nu} S^X_{\mu\nu} \quad (6)$$

where X is I or IJ, A denotes atoms, μ and ν run over atomic orbitals. q^{IJ}_I and q^I_I are the total charges of I in dimer IJ and monomer I, respectively. Z_{I} is the number of protons in I and P^X_A are the Mulliken atomic populations. $\mathbf{D}^X$ and $\mathbf{S}^X$ are the electron density and overlap integrals of X, respectively.

Mulliken charges were criticized in the past[78] and compared to other charge schemes.[79] Gao et al.[80] presented a pictorial representation of the differences in the potentials in eqs 3 and 5 and showed that the field from Mulliken charges deviates considerably from the exact one. Also, Dahlke and Truhlar[81] studied the effect of point charges upon the properties of water clusters in their electrostatically embedded method equivalent to the fixed point charge representation of ESP in FMO.

The main drawback of the Mulliken charges is their instability with respect to an increase in the size of the basis set. In a large basis set, especially with diffuse functions, there are many ways to express a given charge distribution, and the optimal one may be determined variationally. In another basis set, with a different set of exponents, a similar electron density may be optimally represented by a different set of point charges. This ambiguity increases with the size of the basis set, and it can result in very different and basis set-dependent point charges.

The potential-derived charges[82] (often called the ESP charges) are determined by minimizing the figure-of-merit χ^2 in the least-squares procedure:

$$\chi^2(q^{\mathrm{ESP}}) = \sum_{i=1}^{N_{\mathrm{POINTS}}} \left(V^I(\mathbf{r}_i) - \sum_{A\in I}^{N_{\mathrm{ATOMS}}} \frac{q^{\mathrm{ESP}}_A}{|\mathbf{r}_i - \mathbf{R}_A|} \right)^2 \quad (7)$$

$$V^I(\mathbf{r}) = \sum_{A\in I}^{N_{\mathrm{ATOMS}}} \frac{Z_A}{|\mathbf{r} - \mathbf{R}_A|} - \sum_{\mu\nu\in I} D^I_{\mu\nu} \int \frac{\chi_\mu(\mathbf{r}')\chi_\nu(\mathbf{r}')}{|\mathbf{r} - \mathbf{r}'|} d\mathbf{r}' \quad (8)$$

where $V^I(\mathbf{r})$ is the electrostatic potential of fragment I determined at points i on a grid surrounding it. $V^I(\mathbf{r})$ is the functional form of ESP corresponding to the matrix representation in eq 3. $\chi_\mu(\mathbf{r})$ are real-valued atomic basis functions. Practically, potential-derived charges are found[82] as vector $\mathbf{q}$ by solving the matrix equation $\mathbf{Aq} = \mathbf{B}$, where the matrix $\mathbf{A}$ is given by

$$A_{jk} = \sum_{i=1}^{N_{\mathrm{POINTS}}} 1 / r_{ij} r_{ik}$$

the vector $\mathbf{B}$ is

$$B_k = \sum_{i=1}^{N_{\mathrm{POINTS}}} V^I(\mathbf{r}_i) / r_{ik} \text{ and } r_{ij} = |\mathbf{r}_i - \mathbf{r}_j|.$$

Although the ESP charges are less sensitive to an increase in the basis set, they are known to be conformationally dependent and very loosely defined for the so-called "buried"

atoms (because the charges are optimized to reproduce the potential at the molecular surface, on which the buried atoms exert very little influence). In the FMO formulation, these problems are minor as typically FMO fragments are small and have neither a lot of conformational freedom nor buried charges.

We note that Okiyama et al.[83,84] computed restrained ESP charges for the whole system using FMO by expanding the total electrostatic potential (cf eq 8) in the many-body series similar to eq 1, while we use the fragment-derived charges computed individually for fragments to describe the embedding potential following the point charge approximation in FMO,[71] similar to what Kamiya et al.[13] applied to molecular clusters.

Representing the molecular electron density by a set of point charges dramatically decreases the computational cost of evaluating the Coulomb energy. However, this classical approximation is valid only when the electron densities of interacting systems do not overlap, that is, at large separations. As the intermolecular separation decreases and the electron densities begin to overlap, the nuclei of one fragment become less shielded by their electron density and experience stronger attraction by the electron density of the other fragment. Thus, the real electrostatic interaction is somewhat stronger than that calculated by point charges due to charge penetration. It appears that at equilibrium geometries of many molecular clusters, charge penetration plays a significant role. For example, the charge penetration is about 20% of the total interaction energy in the water dimer and becomes even larger at shorter intermolecular separations.[85]

Charge penetration lowers the classical electrostatic energy of interacting point charges due to the overlap of electronic densities. Stone[86] illustrated the origin of charge penetration by considering the interaction of a hydrogen-like atom with nuclear charge Z with a proton. The electrostatic potential of the electron of a hydrogen-like atom has the form:

$$V(R) = -\frac{1}{R} + \exp(-2ZR)\left(Z + \frac{1}{R}\right) = -\frac{1}{R}[1 - \exp(-2ZR)(1 + ZR)] = -\frac{1}{R}f^{\text{damp}}(2ZR) \quad (9)$$

Thus, the potential of an electron in a hydrogen-like atom differs from the classical charge potential by the damping function $f^{\text{damp}}(R)$. This suggests that in general, the point-charge representation of the electrostatic potential may be corrected for charge penetration by the damping function $f^{\text{damp}}(R)$, which has exponential dependence on the separation R. Introducing a parameter $\alpha = 2Z$, one can rewrite the damping function for the charge potential as:

$$f_1^{\text{damp}}(R) = 1 - \exp(-\alpha R)\left(1 + \frac{\alpha R}{2}\right) \quad (10)$$

A simpler form of the damping function is used for electrostatic interactions between the fragments within the effective fragment potential (EFP) framework:[87]

$$f_2^{\text{damp}}(R) = 1 - \exp(-\alpha R) \quad (11)$$

Although the exponential form of the damping function appears from the shape of the potential of the hydrogen-like atom, it is not necessarily the best in general; also, it is computationally more convenient to evaluate integrals between the electronic density of one fragment and charge-distribution of the other fragments modified by Gaussian-like damping functions.[29]

$$f_3^{\text{damp}}(R) = 1 - \beta \exp(-\alpha R^2) \quad (12)$$

The screening of EFP multipoles acting upon the quantum-mechanical (QM) system is performed in QM/EFP calculations with the damping function given in eq 12.

With the inclusion of the damping function, the electrostatic potential (eq 5) in FMO can be defined as

$$V_{\mu\nu}^X = \sum_{K\neq X}^{N} \sum_{A\in K} \left\langle \mu \left| -\frac{q_A f_A^{\text{damp}}(|\mathbf{r} - \mathbf{R}_A|)}{|\mathbf{r} - \mathbf{R}_A|} \right| \nu \right\rangle \quad (13)$$

These screened potentials in eq 13 are denoted as ESPM and ESPP for Mulliken (M) and potential (P) derived charges, respectively. For a given set of charges, parameters α and β can be determined by minimizing the difference between the quantum-mechanical electrostatic potential and the damped multipolar expansion over a grid of points:

$$\Delta = \sum_{\text{grid}} [V_{\text{ab initio}} - V_{\text{damped multipole}}]^2 \quad (14)$$

In this work we chose to use the Gaussian-like damping function (eq 12) with the universal screening parameters of $\alpha = 1$ and $\beta = 1$ based on our earlier experience with screening multipoles.[74] We found that the values of α between 0.5 and 2.0 work very similarly, with the typical differences in the total energy of several kcal/mol or less, with the exception of FMO/HOP with Mulliken charges, where the differences were as large as dozens of kcal/mol in some cases, driven by the unreliable performance of this combination (HOP + ESPM). Parameter β is set to 1 in order to ensure the complete screening of the charge when $R \rightarrow 0$ (important for the bond detached atoms).

In FMO, we applied the Gaussian-like screening only to the bond detached atoms (see Figure 1), that is, the atoms at which the fragment borders lie and which are duplicated in both fragments. This, in particular, results in the effectively zero distance between the charges to be screened and the electron density distributions which they affect as a part of ESP.

$$f_A^{\text{damp}}(R) = \begin{cases} f_3^{\text{damp}}(R), \text{ if } A \text{ is BDA} \\ 1, \text{ otherwise} \end{cases} \quad (15)$$

It is clear that these charges on BDAs are most affected by the screening. We also tested the effect of screening all point charges (not just those of bond detached atoms) and observed a very small difference of 0.5−1.0 and 0.2 (kcal/mol) for some subsets of polypeptides and water clusters, respectively; thus, we limited screening to the bond detached atoms only. It can be expected that in "normal" geometries, that is, without unphysically short contacts between fragments, this is sufficient, but in some "abnormal" situations, in particular, during molecular dynamics[50] it may be desirable to screen all charges.

The following definitions of the errors are used in the accuracy tests below. The absolute error in the total energy of each system S is computed as

$$\Delta E_S = E_S^{\text{FMO}} - E_S^{\text{ab initio}} \tag{16}$$

The composite error is the average of the errors of α,β-$(ALA)_{10}$ and chignolin.

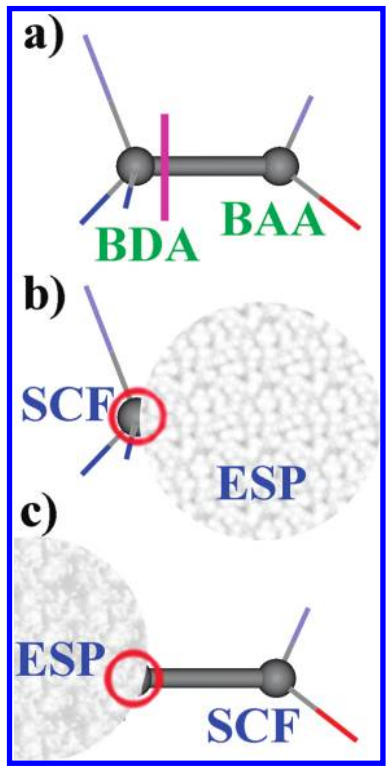

Figure 1. Schematic interfragment border (magenta bar). (a) A bond is detached at the bond detached atom (BDA) on the left, whereas the bond attached atom (BAA) in the right fragment retains this bond. BDA is present in both left and right fragments. (b) In SCF of the left fragment (atoms shown by sticks), the ESP from the right fragment (the hazy sphere) contains contribution from the BDA electron density (or atomic charge) as a part of the right fragment density. (c) Similarly, in SCF of the right fragment, ESP from the left fragment contains contribution from BDA (shown with a red ring).

$$\Delta E_{\text{composite}} = {}^1/_3(|\Delta E_{\alpha-(ALA)10}| + |\Delta E_{\beta-(ALA)10}| + |\Delta E_{\text{chignolin}}|) \tag{17}$$

The error in the isomer energy difference is defined as

$$\Delta E_{\text{isomer}} = |\Delta E_{\alpha-(ALA)10} - \Delta E_{\beta-(ALA)10}| \tag{18}$$

Similar composite and isomer errors are defined for the larger set of systems, α,β-$(ALA)_{20}$ and the Trp-cage miniprotein.

The charge transfer[52] from fragment I to fragment J, ΔQ_{IJ} and the related composite charge transfer amounts[64] used in the error analysis are:

$$\Delta Q_{IJ} = q_I^I - q_I^{IJ} \tag{19}$$

$$\Delta \bar{Q} = \sum_I^N |\sum_{I\neq J}^N \Delta Q_{IJ}| \tag{20}$$

$$\Delta Q = \sum_{I>J}^N |\Delta Q_{IJ}| \tag{21}$$

In eq 19, q_I^I is the total charge of fragment I; q_I^{IJ} is the charge of fragment I within dimer IJ, thus the difference gives the amount of charge of I transferred to J.

As a short-hand notation, we use FMOn/m, where n is 2 (eq 1) or 3 (eq 2) and m is the number of water molecules or residues per fragment.

2.2. Calculation Details. All calculations were performed using Restricted Hartree−Fock (RHF) on the Soroban cluster using modified GAMESS[88] parallelized with the generalized distributed data interface (GDDI).[89] Spherical functions (e.g., 5d) were used throughout. The integral accuracy was increased to 10^{-12}. SCF and SCC convergence thresholds were set to 10^{-7}, except for the 6-311++G** basis set, where both were raised to about 10^{-5} to 10^{-6} to achieve convergence.

The linear dependence deserves a special notion. For large basis sets (namely, those with diffuse functions) there are linear dependent basis functions for chignolin and the Trp-cage miniprotein, which have benzene rings. We used the general means to exclude those linear dependent basis functions by removing those corresponding to the eigenvectors of the overlap

TABLE 1: FMOn Error (kcal/mol) in the Total RHF Energy for Water Clusters Divided into m Molecules Per Fragment, vs ab Initio, for Various Ways to Describe the External Electrostatic Potential (ESP): Mulliken Charges (m), Potential Derived Charges (p), and the Exact 2-Electron Potential (2)[a]

			6-31G*		6-31++G**		cc-pVDZ		aug-cc-pVDZ		cc-pVTZ		aug-cc-pVTZ	
system	m		FMO2	FMO3	FMO2	FMO3	FMO2	FMO3	FMO2	FMO3	FMO2	FMO3	FMO2	FMO3
$(H_2O)_{16}$	1	ESPm	−4.9	0.4	0.6	0.3	−5.5	1.0	3.0	0.7	−5.7	1.4	1.7	0.4
	1	ESPp	−4.6	0.4	0.9	0.3	−9.7	1.0	−1.8	2.0	−7.0	1.3	−0.6	0.9
	1	ESP2	−4.9	0.4	−1.0	0.9	−10.9	1.3	−1.7	−2.7	−9.0	1.7	−7.1	−27.3
	2	ESPm	−2.7	0.2	0.5	0.0	−3.4	0.4	1.5	0.2	−3.2	0.5	0.9	0.0
	2	ESPp	−2.6	0.2	0.6	0.0	−5.3	0.4	−0.6	0.6	−3.9	0.5	−0.2	0.2
	2	ESP2	−2.8	0.2	−0.6	−0.2	−5.9	0.5	−1.2	−0.8	−4.9	0.6	−4.3	−3.6
$(H_2O)_{32}$	1	ESPm	−12.8	1.3	2.2	1.3	−16.3	3.3	6.8	3.1	−16.1	4.4	3.4	1.3
	1	ESPp	−12.0	1.2	3.0	1.3	−25.8	3.5	−5.1	7.9	−18.9	4.3	−2.1	3.4
	1	ESP2	−13.1	1.4	−4.5	2.4	−29.0	4.1	−7.9	−16.0	−24.7	5.8	−28.4	−
	2	ESPm	−8.3	0.4	1.7	0.2	−11.2	0.4	3.7	1.1	−10.0	1.4	1.8	0.2
	2	ESPp	−7.8	0.3	2.3	0.2	−15.8	0.9	−1.5	2.7	−11.2	1.5	−0.7	0.9
	2	ESP2	−8.5	0.4	−3.0	−1.5	−17.6	1.3	−5.0	−430.4	−14.5	2.1	−	−

[a] No potentials are screened. Diverged calculations are shown with "−".

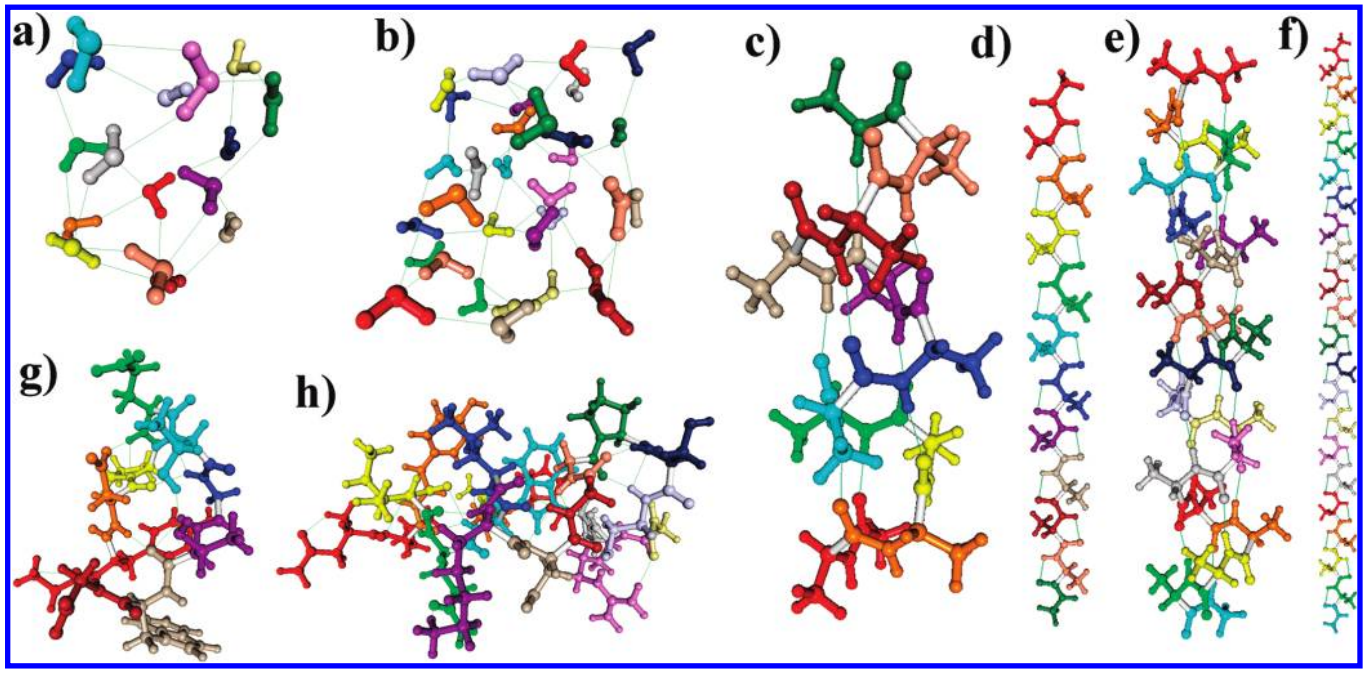

Figure 2. Systems used in tests: (a) $(H_2O)_{16}$, (b) $(H_2O)_{32}$, (c) α-$(ALA)_{10}$, (d) β-$(ALA)_{10}$, (e) α-$(ALA)_{20}$, (f) β-$(ALA)_{20}$, (g) chignolin (1UAO), and (h) Trp-cage miniprotein (1L2Y). Hydrogen bonds are shown with green lines. Fragments (for 1 residue/molecule per fragment division) are depicted in various colors.

matrix with the eigenvalues smaller than a threshold value. Because this technique operates with overlaps of either the whole system (ab initio) or separate fragments, dimers, and trimers (FMO), the removal of linear dependent functions is not exactly the same in FMO and ab initio.

In many cases no linear dependent functions were excluded at all (typically, for STO-3G, 6-31G*, 6-311G*, cc-pVDZ, and cc-pVTZ in polypeptides and for all basis sets in water clusters), whereas in order to obtain convergence some linear dependent functions were eliminated in other cases with the threshold of 10^{-6} (except 6-311++G**, where 10^{-5} was used).

For ESP2, we used the point charge approximation of the field due to far separated fragments with the threshold RESPPC of 2.5 (all distance thresholds are unitless[71] relative to the atomic van der Waals radii; 2.5 typically corresponds to 6.5 Å). Dimer SCF calculations were replaced by the electrostatic approximation[71] with the RESDIM threshold of 3.25. Trimer calculations were neglected[70] if the closest pair in the trimer was separated by more than 1.25 or if the distance to the third fragment from this closest pair was larger than 2.0. In the AFO bond detachment we used the large model with the wide span.[64]

The potential derived charges were computed with the following settings. The charges were constrained to reproduce the molecular charge (water clusters) or charge and dipole moment (polypeptides). The geodesic set of points[90] was used, based on the scaling factor of the van der Waals radii set to 1.4 for the first layer, applied to 4 layers of points with the spacing of 0.2 (in terms of those radii).

3. Results and Discussion

3.1. Water Clusters. The geometries were taken from our previous work,[70] consistent with other accuracy studies. The results are summarized in Table 1. In the following discussion we mainly focus on the cc-pV*l*Z and aug-cc-pV*l*Z basis sets (*l* = D,T) although some results for 6-31G* and 6-31++G** are also given for comparison. Several interesting trends can be discerned. First, when comparing the effect of the diffuse functions, for example, cc-pVDZ versus aug-cc-pVDZ, the latter results for FMO2 are considerably more accurate, with some exceptions for the ESP2 results discussed below. This happens as a net result of two competing effects: (a) larger basis sets have worse results because of the higher order effects involving the exchange-repulsion and charge transfer,[52] (b) larger basis sets (with diffuse functions) have smaller interaction energies, leading to smaller FMO2 errors. The same trend is observed for the comparison of cc-pVDZ and cc-pVTZ, the latter results for FMO2 are more accurate.

The balance of the above two factors for FMO3 is more delicate as the errors themselves are smaller. Apparently, the FMO3 errors for cc-pVDZ are smaller than those for aug-cc-pVDZ. When an ESP based on point charges is used (ESPM or ESPP), for cc-pVTZ vs aug-cc-pVTZ the errors for the larger basis set are smaller, in line with the above trends for FMO2. The most accurate results are obtained for the largest basis set aug-cc-pVTZ.

Comparing 6-31G* and 6-31++G**, one can observe that the latter has a much better accuracy, with a few exceptions limited to FMO3 with ESP2, where the opposite is true. ESPm and ESPp have a similar accuracy for these basis sets, which suggests that the error comes from the many-body quantum effects rather than the description of the electrostatics; this view is supported by the similar but slightly worse accuracy of ESP2 as compared to the other two choices. ESP2 for 6-31++G** does not perform as badly as for aug-cc-pVDZ, which should be related to the extent in which diffuse functions increase the interfragment overlap.

One can also argue that especially FMO2/1 calculations have a smaller basis set superposition error (BSSE) compared to ab initio, because of the reduced extent in which the deficiency in the basis set of monomers is compensated by the basis functions on other fragments, thus some part of the difference in the energies is not an error, but a discrepancy caused by the reduced BSSE. This possibly explains (in part) why smaller basis sets

TABLE 2: FMO*n* Error (kcal/mol) in the Total RHF Energy for the α-Helices and *β*-Strands of $(ALA)_{10}$ and Chignolin (PDB code: 1UAO) Divided into *m* Residues Per Fragment, vs ab Initio, for Various Ways to Describe the External Electrostatic Potential (ESP): Mulliken Charges (m), Potential Derived Charges (p), and the Exact 2-Electron Potential (2), as Well As for the Two Ways to Detach Bonds (AFO and HOP)[a]

				STO-3G		6-31G*		6-311G*		cc-pVDZ		6-31++G**	
system	*m*	bond	ESP	FMO2	FMO3	FMO2	FMO3	FMO2	FMO3	FMO2	FMO3	FMO2	FMO3
α- $(ALA)_{10}$	1	AFO	m	−5.6	−0.5	−1.0	0.6	−0.7	0.7	−9.7	0.2	31.5	−0.6
	1	AFO	p	−0.2	0.0	4.4	0.4	5.7	0.7	3.3	0.9	35.5	−0.7
	1	AFO	2	2.3	−0.1	0.3	0.2	−3.3	0.3	−2.6	1.5	−	−
	1	HOP	m	129.5	9.6	99.8	6.4	90.7	5.7	90.3	5.7	−	−
	1	HOP	p	7.0	1.1	7.5	1.7	5.0	1.6	5.5	2.4	9.1	0.7
	1	HOP	2	−0.1	−0.1	−4.7	0.2	−14.7	−1.9	−12.2	1.2	−	−
	2	AFO	m	0.4	0.0	0.3	0.2	−1.0	0.2	−1.3	0.0	4.0	0.1
	2	AFO	p	0.2	0.0	0.4	0.0	0.5	0.0	0.1	0.1	5.5	0.0
	2	AFO	2	0.2	0.1	−0.8	0.0	−1.8	0.1	−1.7	0.2	−	−
	2	HOP	m	1.8	1.9	4.4	1.6	2.5	1.3	−2.8	1.0	−	−
	2	HOP	p	−0.9	0.3	0.2	0.3	0.1	0.3	−1.0	0.4	2.1	0.4
	2	HOP	2	−0.2	0.1	−1.1	0.0	−5.5	0.0	−3.4	0.2	−	−
β- $(ALA)_{10}$	1	AFO	m	1.0	−0.1	5.3	0.4	11.2	0.9	0.6	0.2	36.3	0.0
	1	AFO	p	2.6	0.2	7.3	0.6	7.1	0.5	6.9	0.9	40.0	0.3
	1	AFO	2	3.0	0.1	−0.1	−0.2	−5.3	−0.6	0.0	0.1	−	−
	1	HOP	m	163.1	31.3	164.3	35.5	183.4	38.7	180.9	38.8	−	−
	1	HOP	p	13.9	3.8	10.9	3.7	9.2	3.2	18.9	5.6	11.0	3.3
	1	HOP	2	0.2	0.0	−6.6	−0.1	−11.2	0.1	−6.1	0.0	−	−
	2	AFO	m	−0.3	0.0	−0.4	0.0	−0.1	0.0	−0.5	0.0	−0.5	0.0
	2	AFO	p	0.0	0.0	0.2	0.0	0.2	0.0	0.3	0.0	0.0	0.0
	2	AFO	2	0.0	0.0	0.1	0.0	0.2	0.0	0.2	0.0	−	−
	2	HOP	m	11.5	1.3	10.8	1.4	11.2	1.5	12.3	1.7	−	−
	2	HOP	p	1.2	0.1	1.1	0.1	1.0	0.1	1.7	0.2	0.9	0.1
	2	HOP	2	0.0	0.0	0.0	0.0	0.1	0.0	0.1	0.0	−	−
1UAO	1	AFO	m	−0.4	−0.4	0.6	0.2	1.8	0.9	−2.1	0.3	56.7	−0.7
	1	AFO	p	2.1	−0.1	8.1	0.3	8.3	0.6	8.0	0.5	61.3	−0.1
	1	AFO	2	3.1	−0.1	2.3	0.1	−11.1	−2.0	0.9	0.5	−	−
	1	HOP	m	157.9	19.6	136.0	18.4	141.8	18.9	129.6	18.3	−	−
	1	HOP	p	9.9	1.9	8.6	2.4	5.8	2.5	11.4	3.6	10.8	1.8
	1	HOP	2	0.5	0.0	−4.8	0.3	−15.6	2.2	−8.2	0.8	−	−
	2	AFO	m	0.9	−0.1	0.4	0.0	−0.2	−0.1	0.8	−0.1	9.6	0.0
	2	AFO	p	0.5	0.0	1.5	0.0	1.7	−0.1	1.8	0.0	8.7	0.0
	2	AFO	2	0.4	0.0	0.3	0.0	0.0	−0.1	0.2	0.0	−	−
	2	HOP	m	16.5	1.5	15.1	2.1	17.2	2.1	15.5	2.3	−	−
	2	HOP	p	1.5	0.3	1.8	0.3	1.4	0.2	2.5	0.5	2.6	0.1
	2	HOP	2	0.3	0.0	0.1	0.0	−2.5	0.1	−0.6	0.1	−	−

[a] No potentials are screened. Diverged calculations are shown with "−".

had a larger error as computed by eq 16. Some explicit ways to correct for BSSE in the FMO framework were developed.[13,91,92]

Mulliken charges are formal, based on the centers at which atomic orbitals are put, disregarding the actual charge distribution, whereas potential-derived charges on the contrary are space-based. This in particular produces a large difference when comparing the accuracy of ESPM and ESPP for the basis sets with diffuse functions. ESPP for all basis sets (except 6-31++G**) and ESP2 results for 6-31G*, cc-pVDZ, and cc-pVTZ have a distinct trend that FMO2 errors are negative while FMO3 errors are positive, while ESPM results appear irregular. This, together with the errors in the dipole moment (not shown) suggests that the latter results reflect some fortuitous error cancellation.

The performance of the exact potential (ESP2) is in all cases worse than the point charge description. This is because the wave functions of fragments are not orthogonal, and the two-electron terms in the potential have no terms describing the exchange-repulsion and charge-transfer effects. This problem gets worse with the basis set increase, resulting in a collapse in some cases, for example, for $(H_2O)_{32}$ with FMO3/aug-cc-pVDZ the error is very large. This is in fact caused by a single trimer, which under the influence of ESP2 converged to an unphysical electronic state with the Mulliken charge of one of the hydrogens of −3.5 e. In other cases no convergence is reached, and the problems of ESP2 get magnified as the interfragment distance becomes shorter. The Q criteria (eqs 20 and 21) can be used together with the ΔQ_{IJ} values (all of them can be extended to trimers for FMO3 diagnostics) to discern manually or automatically such problems.

These ESP2 problems in molecular clusters are less severe than in polypeptides, as described below. Although ESP2 is the exact potential of the Coulomb interaction between the electronic densities, the corresponding exchange interaction described by the exchange operator[72] is absent, and it cannot be added to improve the Coulomb terms because of the nonorthogonality of the fragment wave functions. On the other hand, as shown below for covalently bonded fragments, the point charge description suffers from the short-range problem.

Finally, we observe that doubling the fragment size typically reduces the error by a factor of 2−3. At the best level of FMO3/2 with ESPP, most errors for water clusters are below 1 kcal/mol, although for aug-cc-pVDZ and cc-pVTZ they are 2.7 and 1.5 (kcal/mol), respectively, and a further increase in the fragment size may be needed to lower the error bar more.

3.2. Application to Polypeptides. The geometries of the α-helices and *β*-strands of polyalanine containing 10 and 20

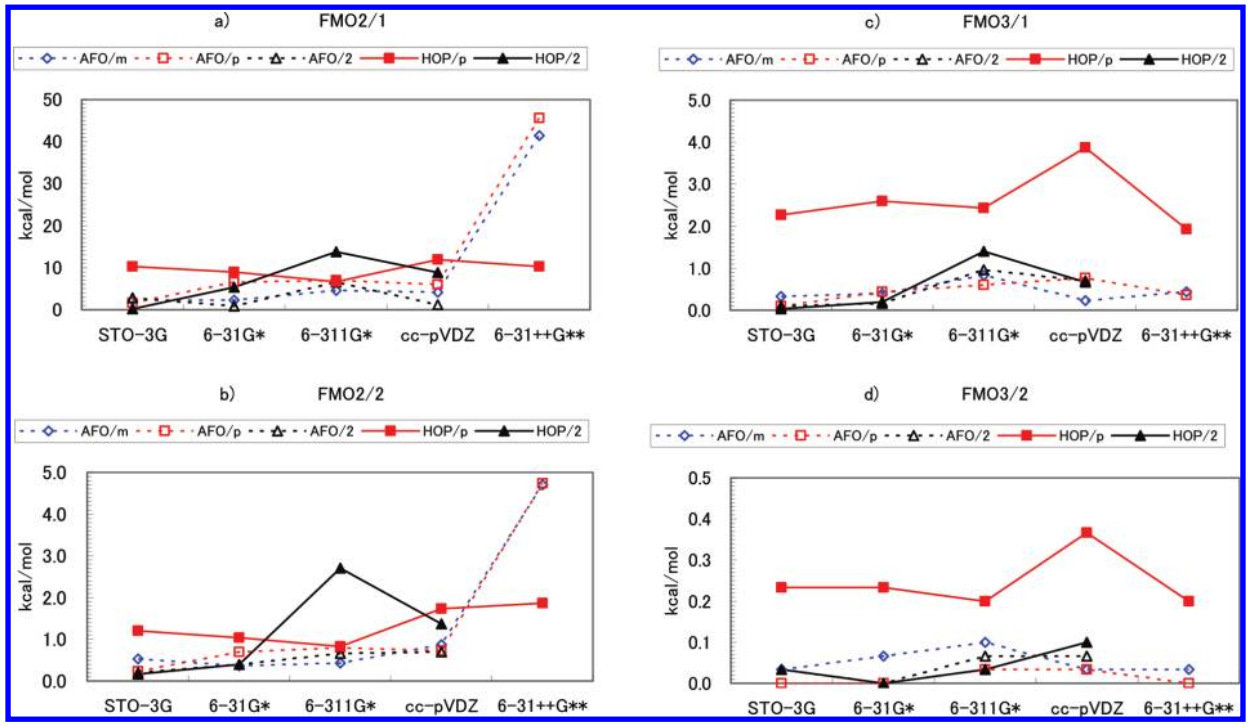

Figure 3. Composite errors in the total RHF energy vs ab initio averaged over α,β-$(ALA)_{10}$ and chignolin, shown for FMO*n*/*m*, where *n* is the many-body expansion level for *m* residues per fragment. (a) FMO2/1, (b) FMO2/2, (c) FMO3/1, and (d) FMO3/2. AFO and HOP bond detachment schemes are depicted as dashed and solid lines, respectively. The Mulliken (ESPm, denoted m here) and potential-derived (ESPp, denoted p here) charge representations are shown as diamonds and squares, respectively. The 2e representation (ESP2) is depicted with triangles. No potentials are screened.

residues capped at both termini were taken from the previous study,[70] denoted by α or β-$(ALA)_n$, $n = 10$ and 20. The chignolin (PDB code: 1UAO) geometry was optimized at the FMO-RHF/MM/6-31(+)G* level, where MM describes solvating water (TIP3P[93]).[44] The Trp-cage geometry was optimized at the FMO-RHF/PCM/6-31(+)G* in the previous study,[94] and this structure differs from the one used in other accuracy studies.[76] (+) indicates that diffuse functions were added to carboxyls only. All structures are shown in Figure 2, drawn using Facio.[95]

Initially, we do not perform screening of ESP, and use the smaller set of systems, $(ALA)_{10}$ (112 atoms, 10 residues, all neutral) and chignolin (138 atoms, 10 residues, 4 of them charged), for a comprehensive test of various representations of ESP, summarized in Table 2. Comparison of the α-helix and β-strand isomers is important to evaluate the accuracy of the relative energetics, eq 18. Chignolin tests are important as a prototype protein study, with four charged residues. The errors are visualized in Figure 3.

Our primary concern in this work is to analyze the origin of the sizable errors of FMO when large basis sets are used[70,76] and to suggest ways to improve the accuracy. Traditionally, FMO was used with the exact representation of the embedding potential (ESP2) and the HOP scheme. It is clear that HOP/ESPM shows unacceptably large errors (exceeding 100 kcal/mol for FMO2/1), which means that the Mulliken point charge representation of ESP fails to work with the HOP scheme, and we therefore omit this level from further discussions, unless otherwise indicated. The AFO scheme, on the other hand, gives reasonable results, because the charges on the fragment borders are largely determined by the frozen orbitals fixed in SCF.

Results in Table 2 and Figure 3 show that for the smallest basis sets STO-3G, HOP/ESP2 is overall the best, with the errors being less than 0.5 kcal/mol among α,β-$(ALA)_{10}$ and chignolin, even at the cheapest level FMO2/1. ESP2 for the double-ζ with polarization basis sets (6-31G* and cc-pVDZ) when compared at all levels works better than either ESPM or ESPP, although some errors like −12.2 kcal/mol in α-$(ALA)_{10}$ with cc-pVDZ are substantial (in which case ESPP gave a considerably better result). AFO/ESP2 has much smaller errors than HOP/ESP2 and is the most accurate at the FMO2 level for 6-31G* and cc-pVDZ.

For the triple-ζ basis set with polarization 6-311G* and in particular for FMO2/1, ESP2 gives rather poor results when HOP is used. For AFO the errors of the three schemes (ESPM, ESPP, and ESP2) were of somewhat comparable accuracy, without a distinct preference.

For 6-31++G**, which has diffuse functions, ESP2 as well as HOP/ESPM fail to give convergence. Otherwise, the errors are in general quite larger and one needs to go beyond FMO2/1 to obtain reasonable results, in which case ESPP and ESPM perform about equally well for the AFO scheme, and for HOP/ESPP the FMO2 and FMO3 errors are smaller and larger than the corresponding AFO/ESPP values, respectively.

Summarizing these results, we conclude that ESP2 can continue to be used with basis sets like 6-31G* or smaller, while the point charge representations outperform it for larger basis sets, which is related to the nonorthogonality of the fragment wave functions, whose overlap increases with the basis set size.

Next, we examine if the results are improved by the screening, whose effect is shown in Table 3 and Figure 4. HOP/ESP2 clearly delivers the worst results for 6-311G*, except FMO3/2 when it is neither the worst nor the best method. On the other hand, AFO/ESPP is consistently the best in accuracy. The effect of screening is overall positive, with the errors decreasing a little, except HOP/ESPP in FMO3, where the opposite is true. For FMO3, the screening approximately halved the HOP/ESPM errors.

TABLE 3: FMO*n* Error (kcal/mol) in the Total RHF Energy for the Shown Systems, Divided into *m* Residues Per Fragment, vs ab Initio, for Mulliken (M) and Potential Derived Charges (P) Representing the External Electrostatic Potential (ESP), As Well As for the Two Ways to Detach Bonds (AFO and HOP)[a]

				6-31G*		6-311G*	
system	*m*	bond	ESP	FMO2	FMO3	FMO2	FMO3
α-$(ALA)_{10}$	1	AFO	M	−1.5	0.5	−1.3	0.7
	1	AFO	P	−0.1	0.3	−0.3	0.4
	1	AFO	2	0.3	0.2	−3.3	0.3
	1	HOP	M	43.1	5.1	43.4	4.1
	1	HOP	P	6.6	2.3	2.2	1.9
	1	HOP	2	−4.7	0.2	−14.7	−1.9
	2	AFO	M	0.5	0.2	−1.0	0.2
	2	AFO	P	0.8	0.0	0.1	0.0
	2	AFO	2	−0.8	0.0	−1.8	0.1
	2	HOP	M	2.2	1.0	0.3	0.9
	2	HOP	P	0.6	0.4	−0.4	0.4
	2	HOP	2	−1.1	0.0	−5.5	0.0
β-$(ALA)_{10}$	1	AFO	M	4.5	0.4	11.0	0.9
	1	AFO	P	1.7	0.4	1.2	0.3
	1	AFO	2	−0.1	−0.2	−5.3	−0.6
	1	HOP	M	55.9	16.1	75.6	21.6
	1	HOP	P	5.7	4.5	3.2	3.8
	1	HOP	2	−6.6	−0.1	−11.2	0.1
	2	AFO	M	−0.4	0.0	−0.1	0.0
	2	AFO	P	0.1	0.0	0.1	0.0
	2	AFO	2	0.1	0.0	0.2	0.0
	2	HOP	M	6.3	0.8	7.7	1.1
	2	HOP	P	1.5	0.2	1.2	0.2
	2	HOP	2	0.0	0.0	0.1	0.0
1UAO	1	AFO	M	0.2	0.2	1.1	0.9
	1	AFO	P	4.2	0.2	0.8	0.6
	1	AFO	2	2.3	0.1	−11.1	−2.0
	1	HOP	M	53.0	8.1	59.3	10.2
	1	HOP	P	8.0	2.8	0.7	3.0
	1	HOP	2	−4.8	0.3	−15.6	2.2
	2	AFO	M	0.6	0.0	−0.2	−0.1
	2	AFO	P	1.8	0.0	0.2	−0.1
	2	AFO	2	0.3	0.0	0.0	−0.1
	2	HOP	M	8.1	0.9	8.3	0.9
	2	HOP	P	2.4	0.3	0.0	0.2
	2	HOP	2	0.1	0.0	−2.5	0.1

[a] All ESPM and ESPP potentials are screened.

Also, the screening approximately halved many of the relatively large FMO2/1 errors for AFO/ESPP, which can be seen by comparing Tables 2 and 3. For instance, the error of 8.1 kcal/mol (1UAO, 6-31G*, Table 2) is reduced to 4.2 kcal/mol (Table 3), and the trend of the error reduction by the screening appears to be general, as can also be seen in Figure 4 (6-311G*) for the composite errors (AFO/p vs AFO/P; ESPp and ESPP, without and with the screening, respectively). When the screening is used for 6-31G*, AFO/ESPP gives comparable but somewhat larger errors than AFO/ESP2, suggesting that the exact potential outperforms point charges for this basis set (provided AFO is used). HOP/ESPP results had large errors, especially for FMO3 (on the relative scale).

Consequently, we examine the size dependence of the errors by looking at the set of systems, $(ALA)_{20}$ (212 atoms, 20 neutral residues) and the Trp-cage miniprotein (304 atoms, 20 residues, 5 of them charged). The results are given in Table 4 and Figure 5, where all point charged potentials are screened. In the 6-311G* calculations, potential derived charges (ESPP) outperform the Mulliken charges (ESPM) and ESP2; whereas AFO/ESPP results are apparently the best. For 6-31G* ESP2 is in general the best, and AFO/ESP2 gives the best results overall. Again, HOP/ESPP showed poor performance.

Finally, we test the accuracy of large basis sets. The results are summarized in Table 5, where AFO/ESPP was used throughout and we note that AFO/ESPM failed to converge in a number of cases, which is probably related to the worse performance of the Mulliken charges for basis sets with diffuse functions. The FMO2 errors are quite large. Here, screening can also be seen to have a positive influence, although typically not very considerable.

One should note that the errors in the energy are affected by various factors, and in some cases these factors cancel out fortuitously, as the very small error for cc-pVTZ in Table 5, 1.0 kcal/mol for FMO2/1 of α-$(ALA)_{10}$. It is, however, in most cases easy to check if the good agreement is fortuitous or not, by looking at the errors in the dipole moment, which in our experience proved to be a reliable indication. We monitored the errors in the dipole moments and used them as an additional guide in forming conclusions, although we did not include the numeric data in this work. For the above quoted error of 1.0 kcal/mol, the error in the FMO2 dipole moment without and with the screening is nearly the same, and the corresponding errors in the energy are 1.0 and −15.7 and kcal/mol, respectively, which indicates that the small error for the former is fortuitous.

Overall, we conclude that for the whole range of basis sets the best set of results is delivered by the FMO/AFO method with the screened ESPP. This is shown in Table 6, which summarizes data from other tables and some additional results (for cc-pVDZ). It is clear that basis sets with diffuse functions need FMO3 for reasonable accuracy, and, except 6-31++G**, two residues are to be assigned per fragment. Also, the optimum scheme of constructing the frozen orbitals in FMO/AFO was determined for smaller basis sets and may need to be revised for larger ones.

Consistent with the earlier results,[76] we observe that AFO typically has a positive error (the AFO absolute energy is above the ab initio value). The observed trends in the errors can be summarized as follows. FMO/HOP is fully variational (i.e., no restriction to the fragment electronic states), and with ESP2 it exactly reproduces ab initio electrostatics (including the polarization; up to the full order N, where N is the number of fragments), which is attractive (lowers the total energy).[52] On the other hand, FMO*n* limits the charge transfer and exchange to the order n (i.e., $n = 2$ or 3). The exchange-repulsion has the repulsive effect of raising the total energy.

This balances out reasonably well for basis sets up to about double-ζ with polarization, and for larger basis sets the polarization (as defined in EDA[32]) outweighs the other terms, resulting in the negative errors of HOP/ESP2 for FMO2 (when no constraint like that of AFO is imposed, see also data for water clusters above). The distinction between the polarization and charge transfer in EDA (and hence in FMO) becomes fuzzy as the basis set size increases. This can be understood by considering the polarization as the intramolecular charge transfer, which for extended basis sets becomes indistinguishable from the intermolecular charge transfer (which is the charge transfer in EDA).

Now, AFO introduces a restriction reducing the polarization, which appears to work well for polyalanines, but shows a positive error of several kcal/mol or even more in some cases for proteins (see also ref 76). This is because the polarization restriction does not correspond to a particular order in the many-body effects.

On the other hand, the PIEDA total energy introduced earlier (eq 34 in ref 52) has a systematic means of limiting the many-body electrostatic effects (by virtue of using the PL0 state), resulting in quite accurate total energies. However, the singly polarized PL0 state can only be unambiguously defined for molecular clusters, whereas for systems such as peptides it relies on a definition of the free state of fragments. In addition, the

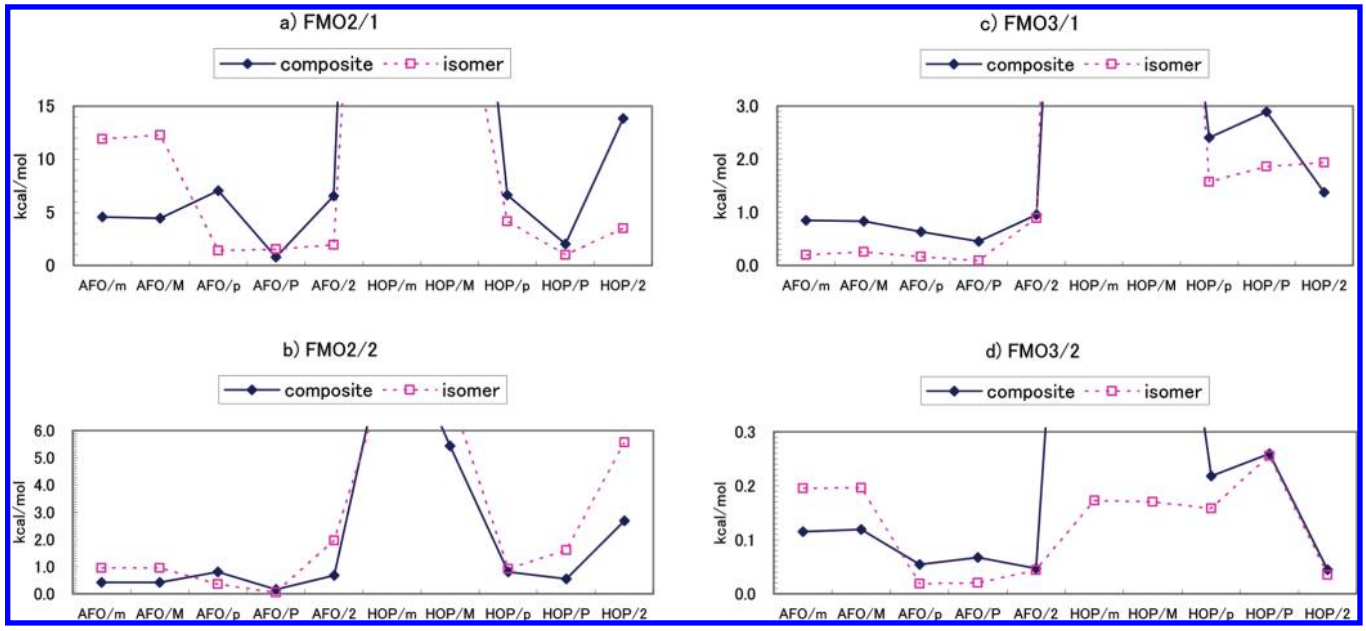

Figure 4. Errors in the total RHF energy vs ab initio for FMO*n*/*m*, where *n* is the many-body expansion level for *m* residues per fragment. (a) FMO2/1, (b) FMO2/2, (c) FMO3/1, and (d) FMO3/2. The composite errors (averaged over α,β-$(ALA)_{10}$, chignolin) and isomer errors (α vs β-$(ALA)_{10}$) are shown as solid and dashed lines, respectively. 6-311G* is used throughout. The treatment of the potential representations is shown as AFO/*k* or HOP/*k*, where *k* is m (ESPm, no screening), M (ESPM, with screening), p (ESPp, no screening), P (ESPP, with screening) and 2 (ESP2).

TABLE 4: FMO*n* Error (kcal/mol) in the Total RHF Energy for the Shown Systems, Divided into *m* Residues Per Fragment, vs ab Initio, for Various Ways to Describe the External Electrostatic Potential (ESP): Mulliken Charges (M), Potential Derived Charges (P), and the Exact 2-Electron Potential (2); As Well As for the Two Ways to Detach Bonds (AFO and HOP)[a]

				6-31G*		6-311G*	
system	*m*	bond	ESP	FMO2	FMO3	FMO2	FMO3
α-$(ALA)_{20}$	1	AFO	M	−6.1	0.1	−6.5	0.7
	1	AFO	P	−0.8	0.6	−1.6	1.1
	1	AFO	2	−0.6	−0.2	−9.4	−0.6
	1	HOP	M	102.2	20.2	107.6	21.0
	1	HOP	P	14.6	7.3	4.6	6.6
	1	HOP	2	−11.6	−0.1	−38.0	−5.4
	2	AFO	M	0.5	0.5	−3.3	0.4
	2	AFO	P	2.0	0.1	0.1	0.1
	2	AFO	2	−2.6	0.1	−5.6	0.1
	2	HOP	M	7.0	4.9	2.8	4.6
	2	HOP	P	1.2	1.5	−1.6	1.6
	2	HOP	2	−3.1	0.0	−16.0	−0.2
β-$(ALA)_{20}$	1	AFO	M	9.3	0.6	24.6	2.3
	1	AFO	P	4.0	1.1	2.9	0.9
	1	AFO	2	−0.1	−0.3	−11.5	−1.4
	1	HOP	M	132.9	44.4	183.5	61.5
	1	HOP	P	14.5	11.9	8.6	10.0
	1	HOP	2	−14.6	−0.2	−24.8	0.4
	2	AFO	M	−1.1	−0.1	−0.2	0.1
	2	AFO	P	0.4	0.1	0.3	0.1
	2	AFO	2	0.2	0.0	0.5	0.1
	2	HOP	M	18.3	3.8	22.8	5.0
	2	HOP	P	4.2	0.9	3.6	0.7
	2	HOP	2	0.0	0.0	0.2	0.1
1L2Y	1	AFO	M	−4.8	0.1	−5.3	1.1
	1	AFO	P	5.3	0.8	0.4	1.3
	1	AFO	2	3.0	0.1	−13.5	−5.5
	1	HOP	M	111.8	23.0	124.7	27.6
	1	HOP	P	16.6	7.1	4.8	7.2
	1	HOP	2	−12.0	−0.2	−37.7	0.0
	2	AFO	M	−0.6	0.0	−5.5	−0.1
	2	AFO	P	1.3	0.1	−1.7	0.0
	2	AFO	2	−1.2	0.0	−4.9	0.0
	2	HOP	M	7.1	1.7	3.3	2.1
	2	HOP	P	0.9	0.4	−2.3	0.5
	2	HOP	2	−1.8	0.1	−9.9	−0.2

[a] All ESPM and ESPP potentials are screened.

PIEDA energy was shown to be accurate for 6-31G*, and for larger basis sets the many-body charge transfer and exchange-repulsion can be expected to become unbalanced, possibly improvable with ESPP, but the extent of the error is unclear at this point. Another promising means to balance the many-body treatment of the electrostatics, exchange-repulsion, and charge transfer is given by the diagrammatic treatment of the FMO energy expansion with the aid of the Green's functions.[96]

When point charges are used (ESPP), apparently the problem of the nonorthogonality of the fragment wave functions is alleviated to some extent, which is on the contrary aggravated by using the exact ESP (ESP2). On the other hand, point charges at short distances cause a very strong polarization of the electronic state, effectively reduced by the screening.The screened HOP/ESPP, which is variational, does not give good results, as seen in various Tables, for example, in Table 4 (while HOP/ESPM is a clear failure). Alarmingly, FMO3 results for HOP/ESPP are sometimes worse than those of FMO2. ESPM in general gave less reliable results than ESPP in the polypeptide systems, as well as for water clusters.

Thus, we conclude that the point charges have to be (a) potential-derived and (b) constrained with AFO, in addition to (c) being screened (in AFO, the molecular orbitals describing the bond spanning several atoms around it are frozen, which largely but not completely determines the atomic charges for BDA and other neighboring atoms). The third mentioned factor (screening) gives a substantial improvement in the accuracy as well. It should be noted that in a number of cases (Table 5) the errors with screening were larger than without, which we attribute mainly to error cancellation, although more tests may be needed for a more definite evaluation.

There is yet another important consideration. As discussed in the previous work (see especially Figure 2 in ref 70), the FMO*n* energy expansion strongly relies on the exact cancellation of the terms in the many-body expression ($n > 1$). In particular, the electrostatic field is added to both monomers and dimers, and the marvel of the FMO energy expression is that each pair electrostatic interaction is counted only once. In case of ESP2 without approximations this is exactly satisfied, because the electrostatic interaction in dimers is computed in a consistent

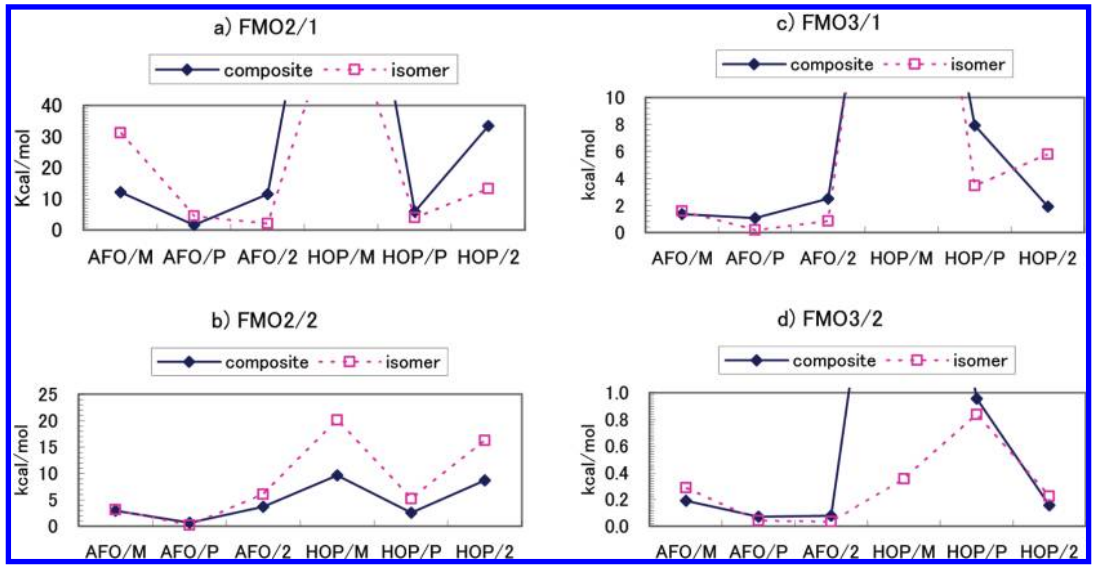

Figure 5. Errors in the total RHF energy vs ab initio for FMO*n*/*m*, where *n* is the many-body expansion level for *m* residues per fragment. (a) FMO2/1, (b) FMO2/2, (c) FMO3/1, and (d) FMO3/2. The composite errors (averaged over α,β-$(ALA)_{20}$, Trp-cage) and isomer errors (α vs β-$(ALA)_{20}$) are shown as solid and dashed lines, respectively. 6-311G* is used throughout. The treatment of the potential representations is shown as AFO/*k* or HOP/*k*, where *k* is M (ESPM, with screening), P (ESPP, with screening), and 2 (ESP2).

TABLE 5: FMO*n* Error (kcal/mol) in the Total RHF Energy for the Shown Systems, Divided into *m* Residues Per Fragment, vs ab Initio, for the Potential Derived Charges Representing the External Electrostatic Potential (ESPP) and the AFO Bond Detachment[a]

			6-31++G**		6-311++G**		aug-cc-pVDZ		cc-pVTZ	
system	*m*	screen	FMO2	FMO3	FMO2	FMO3	FMO2	FMO3	FMO2	FMO3
α-$(ALA)_{10}$	1	no	35.5	−0.7	315.9	14.7	147.5	−12.0	1.0	2.3
	1	yes	27.3	−1.0	319.8	13.0	132.4	−21.8	−15.7	4.4
	2	no	5.5	0.0	74.0	0.2	48.1	0.3	1.4	0.0
	2	yes	3.6	−0.2	75.1	0.2	44.3	0.5	0.2	0.0
β-$(ALA)_{10}$	1	no	40.0	0.3	98.6	0.6	11.4	2.0	4.9	0.5
	1	yes	38.3	0.2	98.7	0.5	−11.2	3.3	−4.1	0.2
	2	no	0.0	0.0	−0.2	0.0	−0.5	0.0	0.2	0.0
	2	yes	−0.2	0.0	−0.5	0.0	−1.7	0.0	0.0	0.0
1UAO	1	no	61.3	−0.1	188.9	4.8	79.3	−0.8	6.9	0.8
	1	yes	54.7	−0.8	183.8	3.7	43.0	−5.8	−5.1	0.4
	2	no	8.7	0.0	36.9	−0.4	12.0	0.3	1.8	−0.1
	2	yes	6.0	−0.1	35.7	−0.8	1.2	1.3	−0.4	−0.2

[a] The usage of the screening of the potentials is shown as yes or no.

TABLE 6: FMO*n* Error (kcal/mol) in the Total RHF Energy for the Shown Systems, Divided into *m* Residues Per Fragment, vs ab initio, for the Potential Derived Charges Representing the External Electrostatic Potential (ESPP) and the AFO Bond Detachment[a]

		6-31G*		6-311G*		cc-pVDZ		6-31++G**		6-311++G**		aug-cc-pVDZ		cc-pVTZ	
system	*m*	FMO2	FMO3	FMO2	FMO3	FMO2	FMO3	FMO2	FMO3	FMO2	FMO3	FMO2	FMO3	FMO2	FMO3
α-$(ALA)_{10}$	1	−0.1	0.3	−0.3	0.4	−2.7	0.6	27.3	−1.0	319.8	13.0	132.4	−21.8	−15.7	4.4
	2	0.8	0.0	0.1	0.0	0.3	0.1	3.6	−0.2	75.1	0.2	44.3	0.5	0.2	0.0
β-$(ALA)_{10}$	1	1.7	0.4	1.2	0.3	0.3	0.6	38.3	0.2	98.7	0.5	−11.2	3.3	−4.1	0.2
	2	0.1	0.0	0.1	0.0	0.2	0.0	−0.2	0.0	−0.5	0.0	−1.7	0.0	0.0	0.0
1UAO	1	4.2	0.2	0.8	0.6	2.8	0.2	54.7	−0.8	183.8	3.7	43.0	−5.8	−5.1	0.4
	2	1.8	0.0	0.2	−0.1	1.9	0.0	6.0	−0.1	35.7	−0.8	1.2	1.3	−0.4	−0.2

[a] All potentials are screened.

fashion: the Coulomb terms in the dimer Fock matrices corresponding to the monomer−monomer electrostatics correspond exactly to the equivalent terms in the ESP added in the monomer Fock matrices (ESP2 with approximations suffers some unbalance problems which were solved to some extent[97]).

However, this cancellation of terms is only approximate in the point charge treatment. To make it easier to understand, consider fragments 1 and 2. The electrostatic interaction between them when individual fragments 1 or 2 are computed, is obtained with the point charge model; however, within dimer 12 this electrostatic interaction is computed with the exact potential as a part of the ab initio internal Fock matrix. This is the origin of some unbalance in the point charge model. However, point charges, especially those based upon the potential, give a close approximation to the exact potential, thus the discrepancy is apparently small.

An important test of the balance of the above effects is to see how the error behaves when the system size increases, as

we conducted in Table 4. The AFO/ESPP appear to be the best, typically having positive errors (its energy being above the ab initio energy). To achieve the chemical accuracy of 1 kcal/mol, the use of FMO3/1 is recommended, unless diffuse functions are present, in which case FMO3/2 is usually required.

As a final remark, we note that a very rough structure can increase the errors manifold, if interfragment distances are very short enlarging the exchange-repulsion and promoting charge transfer. Therefore, care should be exerted in applying FMO (and, most likely, other fragment-based methods) to unrefined structures (or those coming from MD).[48] If such structures have to be used for physical reasons, FMO3 is to be preferred for better energetics.[50] The charge transfer criteria (eqs 20 and 21) or the magnitude of the three-body effects (FMO2 vs FMO3), as well as even the list of interfragment distances can serve as a good test of possible problems.

4. Conclusions

We have performed a systematic study of the embedding electrostatic potential in FMO, using various ways to represent it including the effect of the charge screening, and determined that the exact representation based on the density distribution introduces large errors for large basis sets (triple-ζ with polarization and larger), or/and causes divergence of SCC (basis sets with diffuse functions), attributed to the nonorthogonality of fragment wave functions. We have shown that the two-body FMO has rather large errors when diffuse functions are present and 1 or 2 residues are assigned to one fragment; FMO3 with two residues per fragment is needed for good accuracy.

As a new alternative to the exact potential, we suggest the use of the adaptive frozen orbitals with the screened potential-derived charges, which have been shown to give accurate results for a wide variety of test systems and basis sets. Many properties require diffuse functions in the basis set to get good accuracy, for example, the correlation energy or the dynamic polarizabilities.[98]

In addition to the total energies, the interfragment charge transfer amounts used in the pair interaction energy decomposition analysis (PIEDA)[52] can now be computed using more realistic potential-derived charges rather than the originally proposed Mulliken charges. These atomic charges from FMO calculations have been used in drug design—in scoring functions[99] and in the quantitative structure−activity relationship studies[69]—and the potential-derived charges can be expected to serve as better descriptors. In addition, point charges (ESPM) were used in FMO-NMR[80] to avoid the complication of computing two-electron integrals in ESP over gauge-invariant atomic orbitals, and potential-derived charges can be expected to improve the accuracy of chemical shifts.

Acknowledgment. D.G.F. and K.K. were partially supported by the Next Generation SuperComputing Project, Nanoscience Program (MEXT, Japan). L.V.S. acknowledges support from NSF (CHE-0955419), ACS PRF (49271-DNI6), and Purdue University. D.G.F. and L.V.S. wish to thank Professor Klaus Ruedenberg for the honor and pleasure of the long association with him and many an insightful discussion spanning various branches of science.

References and Notes

(1) Scuseria, G. E. *J. Phys. Chem. A* **1999**, *103*, 4782.
(2) Lee, M. S.; Maslen, P. E.; Head-Gordon, M. *J. Chem. Phys.* **2000**, *112*, 3592.
(3) Werner, H.-J.; Manby, F. R.; Knowles, P. J. *J. Chem. Phys.* **2003**, *118*, 8149.
(4) Nikitina, E.; Sulimov, V.; Zayets, V.; Zaitseva, N. *Int. J. Quantum Chem.* **2004**, *97*, 747.
(5) Choi, C. H. *J. Chem. Phys.* **2004**, *120*, 3535.
(6) Sodt, A.; Subotnik, J. E.; Head-Gordon, M. *J. Chem. Phys.* **2006**, *125*, 194109.
(7) Nakajima, T.; Hirao, K. *Chem. Phys. Lett.* **2006**, *427*, 225.
(8) Paulus, B. *Phys. Rep.* **2006**, *428*, 1.
(9) Anisimov, V. M.; Bugaenko, V. L.; Bobrikov, V. V. *J. Chem. Theory Comput.* **2006**, *2*, 1685.
(10) Inaba, T.; Sato, F. *J. Comput. Chem.* **2007**, *28*, 984.
(11) Stewart, J. J. P. *J. Mol. Mod.* **2009**, *15*, 765.
(12) Sorkin, A.; Dahlke, E. E.; Truhlar, D. G. *J. Chem. Theory Comput.* **2008**, *4*, 683.
(13) Kamiya, M.; Hirata, S.; Valiev, M. *J. Chem. Phys.* **2008**, *128*, 074103.
(14) Rahalkar, A. P.; Ganesh, V.; Gadre, S. R. *J. Chem. Phys.* **2008**, *129*, 234101.
(15) Hua, W.; Fang, T.; Li, W.; Yu, J.-G.; Li, S. *J. Phys. Chem. A* **2008**, *112*, 10864.
(16) He, J.; Di Paola, C.; Kantorovich, L. *J. Chem. Phys.* **2009**, *130*, 144104.
(17) Söderhjelm, P.; Ryde, U. *J. Phys. Chem. A* **2009**, *113*, 617.
(18) Leverentz, H. R.; Truhlar, D. G. *J. Chem. Theory Comput.* **2009**, *5*, 1573.
(19) Suárez, E.; Díaz, N.; Suárez, D. *J. Chem. Theory Comput.* **2009**, *5*, 1667.
(20) Gordon, M. S.; Mullin, J. M.; Pruitt, S. R.; Roskop, L. B.; Slipchenko, L. V.; Boatz, J. A. *J. Phys. Chem. B* **2009**, *113*, 9646.
(21) Mullin, J. M.; Roskop, L. B.; Pruitt, S. R.; Collins, M. A.; Gordon, M. S. *J. Phys. Chem. A* **2009**, *113*, 10040.
(22) Mata, R. A.; Stoll, H.; Cabral, B. J. C. *J. Chem. Theory Comput.* **2009**, *5*, 1829.
(23) Le, H.-A.; Lee, A. M.; Bettens, R. P. A. *J. Phys. Chem. A* **2009**, *113*, 10527.
(24) Huang, L.; Massa, L.; Karle, I.; Karle, J. *Proc. Nat. Acad. Sc. U.S.A.* **2009**, *106*, 3664.
(25) Řezáč, J.; Salahub, D. R. *J. Chem. Theory Comput.* **2010**, *6*, 9199.
(26) Pomogaeva, A.; Gu, F. L.; Imamura, A.; Aoki, Y. *Theo. Chem. Acc.* **2010**, *125*, 453.
(27) Touma, T.; Kobayashi, M.; Nakai, H. *Chem. Phys. Lett.* **2010**, *485*, 247.
(28) He, X.; Merz, K. M., Jr. *J. Chem. Theory Comput.* **2010**, *6*, 405.
(29) Gordon, M. S.; Freitag, M. A.; Bandyopadhyay, P.; Jensen, J. H.; Kairys, V.; Stevens, W. J. *J. Phys. Chem. A* **2001**, *105*, 293.
(30) Xie, W.; Orozco, M.; Truhlar, D. G.; Gao, J. *J. Chem. Theory Comput.* **2009**, *5*, 459.
(31) Kitaura, K.; Ikeo, E.; Asada, T.; Nakano, T.; Uebayasi, M. *Chem. Phys. Lett.* **1999**, *313*, 701.
(32) Kitaura, K.; Morokuma, K. *Int. J. Quantum Chem.* **1976**, *10*, 325.
(33) Fedorov, D. G.; Kitaura, K. *J. Phys. Chem. A* **2007**, *111*, 6904.
(34) (a) Fedorov, D. G.; Kitaura, K., In *Modern Methods for Theoretical Physical Chemistry and Biopolymers*; Starikov, E. B.; Lewis, J. P.; Tanaka, S.; Eds., Elsevier: Amsterdam, 2006; pp 3−38; (b) Nakano, T.; Mochizuki, Y.; Fukuzawa, K.; Amari, S.; Tanaka, S., ibid., pp. 39−52.
(35) *The Fragment Molecular Orbital Method: Practical Applications to Large Molecular Systems*; Fedorov, D. G.; Kitaura, K., Eds.; CRC Press: Boca Raton, FL, 2009.
(36) Fedorov, D. G.; Kitaura, K. *J. Chem. Phys.* **2004**, *121*, 2483.
(37) Fedorov, D. G.; Kitaura, K. *J. Chem. Phys.* **2005**, *122*, 054108.
(38) Fedorov, D. G.; Kitaura, K. *J. Chem. Phys.* **2005**, *123*, 134103.
(39) Mochizuki, Y.; Koikegami, S.; Amari, S.; Segawa, K.; Kitaura, K.; Nakano, T. *Chem. Phys. Lett.* **2005**, *406*, 283.
(40) Maezono, R.; Watanabe, H.; Tanaka, S.; Towler, M. D.; Needs, R. J. *J. Phys. Soc. Jpn.* **2007**, *76*, 064301.
(41) Chiba, M.; Fedorov, D. G.; Kitaura, K. *J. Chem. Phys.* **2007**, *127*, 104108.
(42) Pruitt, S. R.; Fedorov, D. G.; Kitaura, K.; Gordon, M. S. *J. Chem. Theory Comput.* **2010**, *6*, 1.
(43) Auer, B.; Pak, M. V.; Hammes-Schiffer, S. *J. Phys. Chem. C* **2010**, *114*, 5582.
(44) Fedorov, D. G.; Ishida, T.; Kitaura, K. *J. Phys. Chem. A* **2005**, *109*, 2638.
(45) Nagata, T.; Fedorov, D. G.; Kitaura, K.; Gordon, M. S. *J. Chem. Phys.* **2009**, *131*, 024101.
(46) Li, H.; Fedorov, D. G.; Nagata, T.; Kitaura, K.; Jensen, J. H.; Gordon, M. S. *J. Comput. Chem.* **2010**, *31*, 778.
(47) Fedorov, D. G.; Ishida, T.; Uebayasi, M.; Kitaura, K. *J. Phys. Chem. A* **2007**, *111*, 2722.
(48) Komeiji, Y.; Mochizuki, Y.; Nakano, T.; Fedorov, D. G. *J. Mol. Str. (THEOCHEM)* **2009**, *898*, 2.
(49) Fujita, T.; Watanabe, H.; Tanaka, S. *J. Phys. Soc. Jpn.* **2009**, *78*, 104723.

(50) Komeiji, Y.; Mochizuki, Y.; Nakano, T. *Chem. Phys. Lett.* **2010**, *484*, 380.
(51) Mochizuki, Y.; Fukuzawa, K.; Kato, A.; Tanaka, S.; Kitaura, K.; Nakano, T. *Chem. Phys. Lett.* **2005**, *410*, 247.
(52) Fedorov, D. G.; Kitaura, K. *J. Comput. Chem.* **2007**, *28*, 222.
(53) Ishikawa, T.; Mochizuki, Y.; Amari, S.; Nakano, T.; Tokiwa, H.; Tanaka, S.; Tanaka, K. *Theor. Chem. Acc.* **2007**, *118*, 937.
(54) Nakanishi, I.; Fedorov, D. G.; Kitaura, K. *Proteins: Struct., Funct., Bioinf.* **2007**, *68*, 145.
(55) Sawada, T.; Hashimoto, T.; Tokiwa, H.; Suzuki, T.; Nakano, H.; Ishida, H.; Kiso, M.; Suzuki, Y. *Glycoconj. J.* **2008**, *25*, 805.
(56) Watanabe, T.; Inadomi, Y.; Fukuzawa, K.; Nakano, T.; Tanaka, S.; Nilsson, L.; Nagashima, U. *J. Phys. Chem. B* **2007**, *111*, 9621.
(57) Komeiji, Y.; Ishida, T.; Fedorov, D. G.; Kitaura, K. *J. Comput. Chem.* **2007**, *28*, 1750.
(58) Mochizuki, Y.; Komeiji, Y.; Ishikawa, T.; Nakano, T.; Yamataka, H. *Chem. Phys. Lett.* **2007**, *437*, 66.
(59) Sato, M.; Yamataka, H.; Komeiji, Y.; Mochizuki, Y.; Ishikawa, T.; Nakano, T. *J. Am. Chem. Soc.* **2008**, *130*, 2396.
(60) Kistler, K. A.; Matsika, S. *J. Phys. Chem. A* **2009**, *113*, 12396.
(61) Sawada, T.; Fedorov, D. G.; Kitaura, K. *Int. J. Quantum Chem.* **2009**, *109*, 2033.
(62) Ishida, T.; Fedorov, D. G.; Kitaura, K. *J. Phys. Chem. B* **2006**, *110*, 1457.
(63) He, X.; Fusti-Molnar, L.; Cui, G.; Merz, K. M., Jr. *J. Phys. Chem. B* **2009**, *113*, 5290.
(64) Fedorov, D. G.; Avramov, P. V.; Jensen, J. H.; Kitaura, K. *Chem. Phys. Lett.* **2009**, *477*, 169.
(65) Chiba, M.; Fedorov, D. G.; Kitaura, K. *J. Comput. Chem.* **2008**, *29*, 2667.
(66) Taguchi, N.; Mochizuki, Y.; Nakano, T.; Amari, S.; Fukuzawa, K.; Ishikawa, T.; Sakurai, M.; Tanaka, S. *J. Phys. Chem. B* **2009**, *113*, 1153.
(67) Ikegami, T.; Ishida, T.; Fedorov, D. G.; Kitaura, K.; Inadomi, Y.; Umeda, H.; Yokokawa, M.; Sekiguchi, S. *J. Comput. Chem.* **2010**, *31*, 447.
(68) Amari, S.; Aizawa, M.; Zhang, J.; Fukuzawa, K.; Mochizuki, Y.; Iwasawa, Y.; Nakata, K.; Chuman, H.; Nakano, T. *J. Chem. Inf. Comput. Sci.* **2006**, *46*, 221.
(69) Yoshida, T.; Fujita, T.; Chuman, H. *Curr. Comp.-Aided Drug Des.* **2009**, *5*, 38.
(70) Fedorov, D. G.; Kitaura, K. *J. Chem. Phys.* **2004**, *120*, 6832.
(71) Nakano, T.; Kaminuma, T.; Sato, T.; Fukuzawa, K.; Akiyama, Y.; Uebayasi, M.; Kitaura, K. *Chem. Phys. Lett.* **2002**, *351*, 475.
(72) Fedorov, D. G.; Kitaura, K. *J. Chem. Phys.* **2009**, *131*, 171106.
(73) Söderhjelm, P.; Öhrn, A.; Ryde, U.; Karlström, G. *J. Chem. Phys.* **2008**, *128*, 014102.
(74) Slipchenko, L. V.; Gordon, M. S. *J. Comput. Chem.* **2007**, *28*, 276.
(75) Nakano, T.; Kaminuma, T.; Sato, T.; Akiyama, Y.; Uebayasi, M.; Kitaura, K. *Chem. Phys. Lett.* **2000**, *318*, 614.
(76) Fedorov, D. G.; Jensen, J. H.; Deka, R. C.; Kitaura, K. *J. Phys. Chem. A* **2008**, *112*, 11808.
(77) Mulliken, R. S. *J. Chem. Phys.* **1955**, *23*, 1833.
(78) Bayly, C. I.; Cieplak, P.; Cornell, W.; Kollman, P. A. *J. Phys. Chem.* **1993**, *97*, 10269.
(79) Pendás, A. M.; Blanco, M.; Francisco, A. E. *J. Comput. Chem.* **2007**, *28*, 161.
(80) Gao, Q.; Yokojima, S.; Fedorov, D. G.; Kitaura, K.; Sakurai, M.; Nakamura, S. *J. Chem. Theory Comput.* **2010**, *6*, 1428.
(81) Dahlke, E. E.; Truhlar, D. G. *J. Chem. Theory Comput.* **2007**, *3*, 46.
(82) Besler, B. H.; Merz, K. M., Jr.; Kollman, P. A. *J. Comput. Chem.* **1990**, *11*, 431.
(83) Okiyama, Y.; Watanabe, H.; Fukuzawa, K.; Nakano, T.; Mochizuki, Y.; Ishikawa, T.; Tanaka, S.; Ebina, K. *Chem. Phys. Lett.* **2007**, *449*, 329.
(84) Okiyama, Y.; Watanabe, H.; Fukuzawa, K.; Nakano, T.; Mochizuki, Y.; Ishikawa, T.; Ebina, K.; Tanaka, S. *Chem. Phys. Lett.* **2009**, *467*, 417.
(85) Slipchenko, L. V.; Gordon, M. S. *Mol. Phys.* **2009**, *107*, 999.
(86) Stone, A. J. *The Theory of Intermolecular Forces*; Oxford University Press: Oxford, 1996.
(87) Freitag, M. A.; Gordon, M. S.; Jensen, J. H.; Stevens, W. J. *J. Chem. Phys.* **2000**, *112*, 7300.
(88) Schmidt, M. W.; Baldridge, K. K.; Boatz, J. A.; Elbert, S. T.; Gordon, M. S.; Jensen, J. H.; Koseki, S.; Matsunaga, N.; Nguyen, K. A.; Su, S.; Windus, T. L.; Dupuis, M.; Montgomery, J. A., Jr. *J. Comput. Chem.* **1993**, *14*, 1347 GAMESS can be downloaded from: http://www.msg.chem.iastate.edu/gamess/gamess.html.
(89) Fedorov, D. G.; Olson, R. M.; Kitaura, K.; Gordon, M. S.; Koseki, S. *J. Comput. Chem.* **2004**, *25*, 872.
(90) Spackman, M. A. *J. Comput. Chem.* **1996**, *17*, 1.
(91) Ishikawa, T.; Mochizuki, Y.; Nakano, T.; Amari, S.; Mori, H.; Honda, H.; Fujita, T.; Tokiwa, H.; Tanaka, S.; Komeiji, Y.; Fukuzawa, K.; Tanaka, K.; Miyoshi, E. *Chem. Phys. Lett.* **2006**, *427*, 159.
(92) Ishikawa, T.; Ishikura, T.; Kuwata, K. *J. Comput. Chem.* **2009**, *30*, 2594.
(93) Jorgensen, W. L.; Chandrasekhar, J.; Madurs, J.; Impey, R. W.; Klein, M. L. *J. Chem. Phys.* **1983**, *79*, 926.
(94) Li, H.; Fedorov, D. G.; Nagata, T.; Kitaura, K.; Jensen, J. H.; Gordon, M. S. *J. Comput. Chem.* **2010**, *31*, 778.
(95) Suenaga, M. *J. Comput. Chem. Jpn.* **2008**, *7*, 33 (in Japanese). Facio 14.2.2, http://www1.bbiq.jp/zzzfelis/Facio.html.
(96) Yasuda, K.; Yamaki, D. *J. Chem. Phys.* **2006**, *125*, 154101.
(97) Fedorov, D. G.; Kitaura, K. *Chem. Phys. Lett.* **2006**, *433*, 182.
(98) Mochizuki, Y.; Ishikawa, T.; Tanaka, K.; Tokiwa, H.; Nakano, T.; Tanaka, S. *Chem. Phys. Lett.* **2006**, *418*, 418.
(99) Fischer, B.; Fukuzawa, K.; Wenzel, W. *Proteins: Struct., Funct., Bioinf.* **2008**, *70*, 1264.

JP101724P